Radio continuum observations of low mass young stars driving outflows

Rachael Ainsworth, Anna Scaife, Tom Ray & AMI Consortium

Dublin Institute for Advanced Studies

rainsworth@cp.dias.ie, a.scaife@soton.ac.uk, tr@cp.dias.ie

1. Abstract

We present 16 GHz deep radio continuum observations made with the Arcminute Microkelvin Imager (AMI) of a sample of low-mass young stellar objects (YSOs) driving jets. We compile and examine spectral energy distributions (SEDs) for each source using data from an extensive literature search and calculate both radio and sub-mm spectral indices in two different scenarios: (i) fixing the dust temperature according to evolutionary class; (ii) allowing the dust temperature to vary. We use these derived spectral indices to place constraints on the physical mechanisms responsible for the radio emission and find that 80% of the objects in this sample have spectral indices consistent with free-free emission from a partially ionised outflow. We examine correlations between the radio luminosity and bolometric luminosity, envelope mass, and outflow force and investigate the error contributions of different spectral parameters to constraining the radio luminosity of these objects.

2. Introduction

Class 0 protostars represent the youngest phase of protostellar evolution in which the central object has yet to accrete most of its mass from the surrounding envelope, and is therefore less massive than the envelope ($M_{\rm env} > M_*$) [6]. The subsequent Class I phase [8] occurs when the majority of the remainder of the envelope has accreted onto the protostar or its circumstellar disc ($M_{\rm env} < M_*$). Embedded YSOs are often found to have partially ionised and collimated outflows/jets driven by the accretion from their envelopes, detectable at centimetre wavelengths almost certainly via thermal bremsstrahlung radiation. This free-free emission is typically found to have a flat or positive power-law spectral index α, where the flux density $S_\nu \propto \nu^\alpha$ at frequency ν. Unresolved sources can exhibit partially opaque spectra with spectral indices in the range -0.1$\leq \alpha \leq$2, where a value of -0.1 indicates optically thin free-free emission and a value of 2 indicates optically thick. α=0.6 is found for a standard, canonical jet [9].

We present 16 GHz deep radio continuum observations made with AMI of a sample of low-mass YSOs driving known outflows. We investigate the properties of this *total* radio emission and compare it to the clearly defined trends with other global properties of these systems, such as bolometric luminosity ($L_{\rm bol}$), envelope mass ($M_{\rm env}$), and outflow force ($F_{\rm out}$), measured in previous works [2, 3, 4]. We combine our results for the flux densities with those found in an extensive literature search to calculate the spectral indices at radio wavelengths, and find that they are consistent with free-free emission as the mechanism for the radio emission.

3. Results

The AMI 16 GHz combined-channel map for one of the target sources, L1448, is shown in Figure 1, and we measure an integrated flux density of $S_{16\,\rm GHz}$=2.39$\pm$0.16 mJy for this source. Detailed notes on L1448, along with flux densities, maps and notes for the remainder of the sample, can be found in [1].

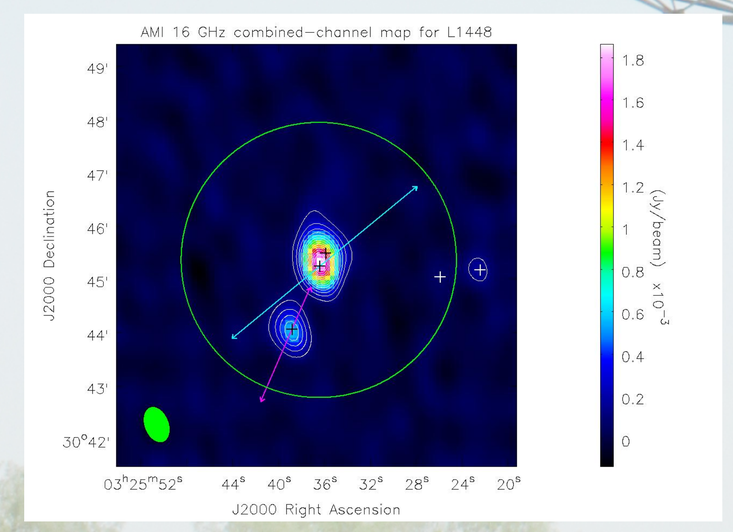

Figure 1: *The AMI 16 GHz combined channel map uncorrected for the primary beam response for L1448. Known protostellar objects (+) are from [7]. Solid lines indicate outflow axes for L1448 NB (cyan) and L1448 C (magenta) from [10]. The primary beam response is shown as a solid circle and the PSF for the dataset as a filled ellipse in the bottom left corner. Contours at 5, 10, 15, 20 $\sigma_{\rm rms}$ etc, where $\sigma_{\rm rms}$=24 μJy beam^{-1}.*

4. SEDs and Spectral Indices

Power-law spectral indices, $\alpha_{\rm AMI}$, were fitted to the AMI channel data alone for each object. 78% of the target sample had $\alpha_{\rm AMI}$ consistent with free-free emission, and the weighted average spectral index is found to be $\overline{\alpha_{\rm AMI}}$=0.42$\pm$0.59, consistent with the value for a canonical jet.

We then fit a combined radio power law, with spectral index α', and blackbody model to the larger data set for each source. This fit utilised data at wavelengths >100 μm collected from an extensive literature search and had the form:

$$S_{\rm total} = S_1 + S_2 = K_1 \left(\frac{\nu}{\nu_1}\right)^{\alpha'} + K_2 \frac{\nu^\beta B_\nu(T_{\rm d})}{\nu_2^\beta B_{\nu_2}(T_{\rm d})}, \quad (1)$$

where β is the dust opacity index, B_ν is the Planck function for a dust temperature $T_{\rm d}$, K_1 is the normalized flux density at ν_1=16 GHz and K_2 is the normalized flux density at ν_2=300 GHz.

Fitting was performed in two scenarios to obtain the maximum likelihood values for α', β, and $T_{\rm d}$ of each source: (i) by fixing $T_{\rm d}$ based on evolutionary class, and (ii) by allowing $T_{\rm d}$ to vary. In both scenarios, 80% of the target sample had α' consistent with free-free emission, and $\overline{\alpha'}$=0.20$\pm$0.4. The SED for L1448 is shown in Figure 2 with the results from (ii) overlaid. The SED results and plots for the remainder of the sample can be found in [1].

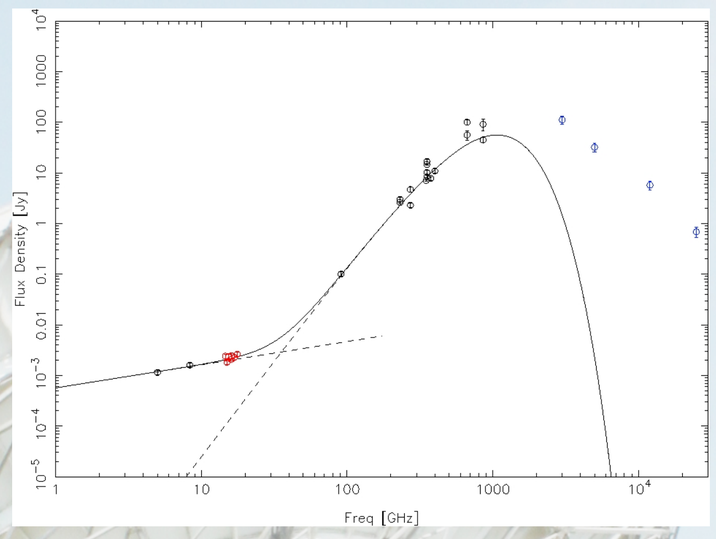

Figure 2: *L1448 SED plotted with Scenario (ii) results. AMI data points are indicated in red. Only data ν <3 THz (λ >100 μm) were included in the fit, but IRAS data ν >3 THz are included in the plot (blue data points) for illustration and could be fitted by a star + disc model.*

5. The Greybody Contribution

At 16 GHz there is expected to be a small contribution to the radio flux density of protostars due to the long wavelength tail of the thermal dust emission from the envelopes around these objects [5]. It is important to separate this component from the free-free emission and we calculate this predicted contribution to the 16 GHz flux density in the following way:

$$S_{\rm gb,16} = f(K_2, \beta, T_{\rm d}) = K_2 \frac{\nu_1^\beta B_{16}(T_{\rm d})}{\nu_2^\beta B_{300}(T_{\rm d})}, \quad (2)$$

with an associated error

$$\sigma^2_{S,16} = \left(\frac{\partial f}{\partial K_2}\sigma_{K_2}\right)^2 + \left(\frac{\partial f}{\partial \beta}\sigma_\beta\right)^2 + \left(\frac{\partial f}{\partial T_{\rm d}}\sigma_{T_{\rm d}}\right)^2, \quad (3)$$

where ν_1=16 GHz, ν_2=300 GHz, and σ_{K_2}, σ_β and $\sigma_{T_{\rm d}}$ are the uncertainties on K_2, β and $T_{\rm d}$ respectively. In all cases the error is found to be dominated by the uncertainty on β. For example, in the case of L1448: $\sigma^2_{S,16} = 4.39^2 \pm 75.8^2 \pm 14.3^2$ μJy.

We subtract $S_{\rm gb,16}$ from the measured 16 GHz flux density to obtain values of only the radio emission due to the outflow component at 16 GHz, $S_{\rm rad,16}$. We compute the radio luminosities, $L_{\rm rad} = S_{\rm rad,16} d^2$ (where d is distance to the source), to use in the correlations that follow. All results can be found in [1].

6. Correlations

$L_{\rm rad}$ has been shown to correlate with global properties such as $L_{\rm bol}$, $M_{\rm env}$, and $F_{\rm out}$, and we find that these new data are broadly consistent with the trends seen in lower luminosity samples [2, 3, 4]. The correlation with $L_{\rm bol}$ is shown in Figure 3, and we find a slight bias towards higher values of $L_{\rm bol}$. The strong correlation of $L_{\rm rad}$ with $M_{\rm env}$ is shown in Figure 4. In Figures 3 and 4, filled circles represent Class 0 sources from this sample, stars are Class I, and unfilled circles are previous data. The correlation with $F_{\rm out}$ along with a detailed discussion of these correlations can be found in [1].

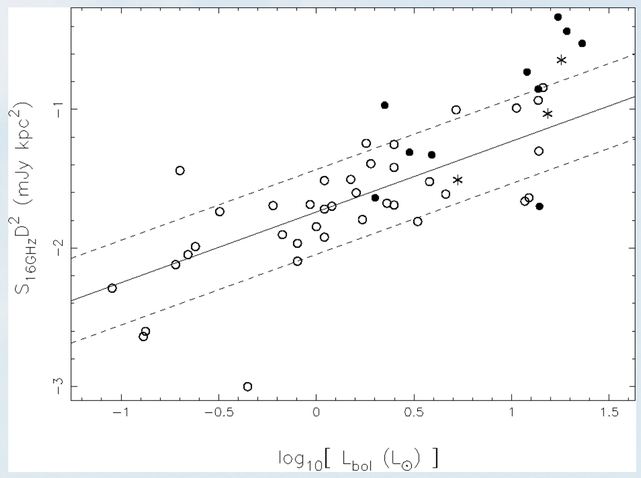

Figure 3: *Correlation of 16 GHz $L_{\rm rad}$ with $L_{\rm bol}$ when $T_{\rm d}$ varies. Best fitting correlation of slope 0.51$\pm$0.26 from [3] is shown as a solid line.*

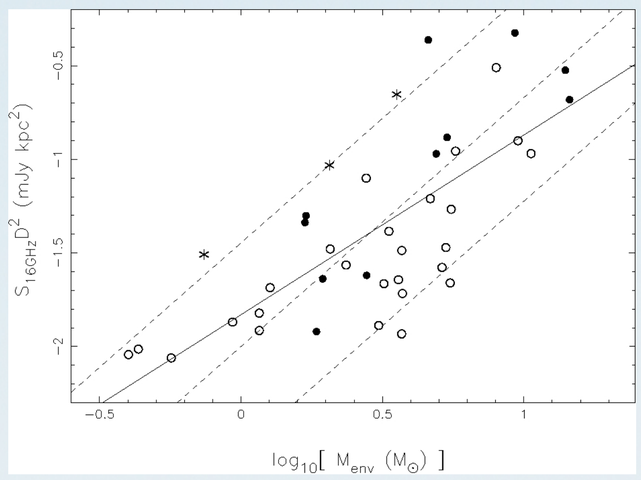

Figure 4: *Correlation of 16 GHz $L_{\rm rad}$ with $M_{\rm env}$, where the solid line indicates the best fitting correlation of slope 0.96$\pm$0.41 using the combined data set, the dashed lines indicate a slope of 1.33 and the 1σ limits on the distribution of data relative to this slope, see [3].*

7. Conclusions

- The data presented in this work provides support for free-free emission as the dominant mechanism for producing $L_{\rm rad}$ from these YSOs. Across the AMI channel bands, 78% of the detected YSOs in this sample have spectral indices $\alpha_{\rm AMI}$ consistent with free-free emission, and we find an average spectral index of $\overline{\alpha_{\rm AMI}}$=0.42$\pm$0.59, consistent with the value for a canonical thermal jet.
- We have presented and examined SEDs for each detected protostellar source, combining the AMI data with available archival data from an extensive literature search. We tested two scenarios to obtain maximum likelihood values for α', β, and $T_{\rm d}$: (i) by fixing $T_{\rm d}$ for each source based on evolutionary class, and (ii) by allowing $T_{\rm d}$ to vary. In both scenarios we find that 80% of the objects in the target sample have α' consistent with free-free emission, and we calculate an average spectral index $\overline{\alpha'}$=0.2$\pm$0.4 consistent with the value for a well-collimated outflow.
- We examine the errors associated with determining $L_{\rm rad}$ at 16 GHz and find that the dominant source of error is the uncertainty on β.
- We examine correlations between $L_{\rm rad}$ and other global properties of these systems, and find that these data are broadly consistent with correlations found in previous samples. We improve the strong correlation with $M_{\rm env}$, and we find a slight bias in the $L_{\rm rad}$–$L_{\rm bol}$ relationship towards higher values of $L_{\rm bol}$.

References

[1] AMI Consortium: Ainsworth, R., et al., 2012, arXiv:1203.3381v1 [astro-ph.SR].

[2] AMI Consortium: Scaife, A., et al., 2011a, MNRAS, 410, 2662.

[3] AMI Consortium: Scaife, A., et al., 2011b, MNRAS, 415, 893.

[4] AMI Consortium: Scaife, A., et al., 2012a, MNRAS, 420, 1019.

[5] AMI Consortium: Scaife, A., et al., 2012b, MNRAS, 420, 3334.

[6] André, P., Ward-Thompson, D., Barsony, M., 1993, ApJ, 406, 122.

[7] Hatchell, J., Fuller, G., Richer, J., Harries, T., Ladd, E., 2007, A&A, 468, 1009.

[8] Lada, C. J., 1987, IAU Symp, 115, 1.

[9] Reynolds, S., 1986, ApJ, 304, 713.

[10] Wolf-Chase, G., Barsony, M., O'Linger, J., 2000, AJ, 120, 1467.